Journal of Applied Electrochemistry **30**: 1285–1292, 2000.
© 2000 *Kluwer Academic Publishers. Printed in the Netherlands.*

Mass transfer in fluidized beds of inert particles. Part I: The role of collision currents in mass transfer to the electrode

N.A. SHVAB[1], N.V. STEFANJAK[1], K.A. KAZDOBIN[1] and A.A. WRAGG[2]
[1]*Institute of General & Inorganic Chemistry, Ukrainian National Academy of Sciences, Palladin Avenue, 32/34, Kiev, 252680, Ukraine*
[2]*School of Engineering and Computer Science, University of Exeter, North Park Road, Exeter, Devon EX4 4QF, Great Britain*

Received 6 July 1999; accepted in revised form 11 January 2000

Key words: collision mechanism, electrode, fluidized bed, mass transfer

Abstract

The effect of particle-wall collision on the mass transfer rate mechanism in liquid fluidized bed electrochemical cells was studied. Collision frequencies and currents were measured at microelectrodes set in the bed wall. It is postulated that, at each particle–electrode collision, a specific microvolume of bulk concentration electrolyte is introduced into the near-electrode diffusion layer during particle movement towards the electrode causing an enhancement of the limiting diffusion current. Based on measurements made at microelectrodes calculations of the contribution of the particle collision mechanism to total mass transfer to a planar electrode are attempted and are in good agreement with experimental values.

List of symbols

A_c	mean of alternating voltage caused by collision currents (V)
c_o	bulk concentration of electroactive species (M)
D	diffusion coefficient ($cm^2\ s^{-1}$)
d_p	average particle diameter (mm)
f	single collision frequency of particles with the electrode (s^{-1})
f_r	collision frequency of particles per unit area of electrode surface ($s^{-1}\ cm^{-2}$)
g	gravitational acceleration ($cm\ s^{-2}$)
H	fluidized bed height (cm)
H_0	static bed height (cm)
h	height of spherical segment, $h = \delta$ (cm)
i_c	integral of collision current density ($mA\ cm^{-2}$)
i_{in}	part of current density caused by interstitial flow ($mA\ cm^{-2}$)
i_d	limiting diffusion current density ($mA\ cm^{-2}$)
i_{mf}, i_d^{max}	limiting diffusion current densities at minimum fluidization and optimum bed expansion, respectively ($mA\ cm^{-2}$)
i_{ec}^{mf}, i_{ec}^{max}	limiting diffusion current densities in empty channel at U_{mf} and L_{opt}, respectively ($mA\ cm^{-2}$)
K_d	mass transfer coefficient ($cm\ s^{-1}$)
L	normalized expansion of the fluidized bed, $L = H/H_o$
L_{opt}	optimal fluidized bed expansion
n_c	number of particles per unit electrode area
R_{met}	measuring resistance (Ω)
r_{eff}	effective particle radius, $r_{eff} = 0.5(d_p + \delta_0)$ (cm)
S_e	electrode surface area (cm^2)
U	electrolyte linear flow velocity ($cm\ s^{-1}$)
U_{in}	interstitial flow velocity ($cm\ s^{-1}$)
U_{mf}	minimum fluidization velocity ($cm\ s^{-1}$)
z	number of electrons

Greek symbols

δ	diffusion boundary layer thickness (cm)
δ_o	hydrodynamic boundary layer thickness (cm)
ε	fluidized bed porosity
ε_o	bed porosity at incipient fluidization, $\varepsilon_o \approx 0.4$
ξ	dimensionless coefficient of hydraulic pressure head
ρ_p	particle density ($g\ cm^{-3}$)
ρ_s	solution density ($g\ cm^{-3}$)
τ_c	particle–electrode contact time (s)

1. Introduction

One of the most efficient methods of diffusion boundary layer disturbance to enhance mass transfer is the use of beds of fluidized inert particles (FIB) [1], in which the solid phase usually consists of spherical glass particles [1, 2]. Electrolysis in FIBs has been successfully applied in electrochemical technology, for example, in nonfer-

rous metal winning from plating wastes [3, 4]. The use of a fluidized bed allows the limiting diffusion current density, i_d, to be increased several times above that for single phase flow alone [5, 6]. This enhancement occurs due both to disturbance of the diffusion boundary layer [1, 2, 6, 7] and the particle-wall collision mechanism [8, 9]. Mass transfer to the electrode in beds of inert particles has been investigated widely on the macrolevel [10–13]. However, the role of particle-wall collisions and also the collision mechanism is not well understood.

Various opinions have been formulated concerning the nature of the FIB effect on electrode processes. On the one hand it has been considered that, at each collision, a definite microvolume of electrolyte is introduced into the near-electrode diffusion layer, thus causing enhancement of the limiting diffusion current [8, 9]. Other authors [14] have played down the influence of collisions on the electrode process rate, explaining the mass transfer increase as due to transition of the flow from laminar to turbulent. Systems of different porosity were investigated. The porosity variation, however, was imitated artificially by accommodation of PVC cylinders or Nylon spheres in the channel. Thus, there were no collision phenomena, the system effectively being a fixed bed. In addition because spheres act as bluff bodies, the flow becomes turbulent at rates corresponding to $Re \leqslant 20$ [6, 7], that is, smaller than the minimum fluidization velocity for such systems.

It was decided to measure collision frequencies and currents under various hydrodynamic conditions in order to confirm earlier suggestions concerning the influence of collisions on mass transfer rates [8, 9].

2. Experimental details

2.1. *Measuring cell and electrodes*

Measurements of collision frequencies and currents at a planar electrode were made by means of an oscilloscopic technique, briefly described in [15] and depicted schematically in Figure 1. The working microelectrode was a platinum wire with its cross-section flush mounted with a vertical Plexiglass plate (the electrode support). The electrode was fixed using epoxy cement and was ground and polished flush with the plate. The microelectrode in its support plate was positioned facing the diaphragm at a height of 10 cm from the flow distributor. The diameter of the microelectrode working surface matched the average diameter of the studied particles. Thus, only one particle could participate in collision with the microelectrode at one time. Exact measurements of the microelectrode surfaces were made using a microscope (MIM-6).

Planar electrodes of 1 or 2 cm^2 were also used for the measurement of limiting currents by the voltammetric method at a scanning rate of 5 mV s^{-1}. These electrodes were manufactured and mounted similarly to the microelectrodes.

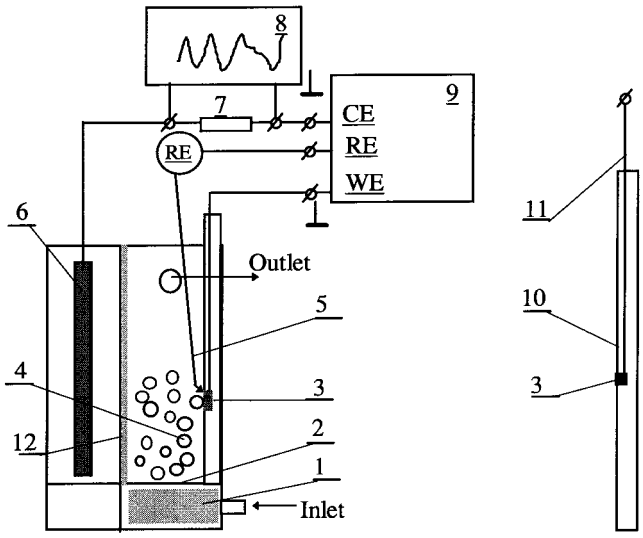

Fig. 1. Electrochemical measurement circuit design. Key: (1) flow distributor; (2) plastic mesh support; (3) microelectrode; (4) fluidized bed particles; (5) Luggin capillary; (6) counter electrode; (7) measuring resistance, R_{met}; (8) oscilloscope; (9) potentiostat; (10) electrode support plate; (11) insulated contact; (12) diaphragm.

To achieve uniform bed fluidization and to minimize entrance effects, a dynamic flow distributor, made of multilayers of plastic mesh containing glass beads, was placed at the bottom of the cell. Narrow size fractions of spherical glass beads of density $\rho_p = 2.5$ g cm^{-3}, and with average diameter in the range $0.5 < d_p < 2.5$ mm were used. Measurements were made in electrolyte of composition, $[Cu^{2+}] = 2$ to 5×10^{-2} M; $[Na_2SO_4] = 1.0$ M; $2.1 < pH < 2.5$, at a temperature of 20 ± 2 °C.

2.2. *Measurement of collision frequencies*

Only a single particle could collide with the microelectrode at one time, whereas previous experiments have involved multiple collisions with the electrodes as a plate [16, 17] or a sphere [18]. In [17, 18] the current pulses resulted from instantaneous conducting bridges of conducting particles of Raney nickel [17] or copper-coated glass spheres [18]. Thus, the collision frequencies found in [16–18] are overestimated. The present method of collision frequency measurement on microelectrodes allows individual collisions to be registered.

2.3. *Measurement of collision currents*

Current pulses, caused by collisions, were calculated from the values of the oscilloscope pulses, produced by voltage changes across the measuring resistance, R_{met}, of 952 Ω, which was incorporated in the counter electrode line (Figure 1). The measuring resistance was screened. The screen was connected to the screen cover of the connecting cable, which was grounded to the P-5848 potentiostat. The signal was sent to the RC-filtered input of a C1–48B oscilloscope ($R = 1$ MΩ, $C = 50$ mF). Thorough protection from noise was necessary due to the very small current pulses caused by individual

collisions. The contribution of parasitic signals to the measured signal values of a current pulse did not exceed 1–3%.

The measurements were carried out in potentiostatic mode at a potential, $E_c = -0.2$ V, at which the limiting diffusion current was reached. A Luggin capillary was placed close to the microelectrode. The lead counter electrode was separated from the working space of the cell by a thermally treated PVC fabric diaphragm. The potential sweep rate of the oscilloscope screen was chosen in order to ensure clear division of the peaks, so that their number did not exceed 6–8 each measurement.

3. Results and discussion

The frequency of particle collisions with the electrode as a function of the bed porosity and particle size was measured. Typical oscilloscope pulse images, as shown in Figure 2, may be interpreted as collisions, rather then hydrodynamically induced fluctuations. This is confirmed by: (i) the absence of characteristic peaks on the oscillogram for measurements in flow without particles, and (ii) by the fact that they were observed only at the limiting diffusion current. The availability of a powerful RC filter on the oscilloscope input also ensured that the registered pulses are not alternating current noise on the microelectrode.

The pulse shape is determined by the type of particle contact with the electrode; firstly a direct (individual) pulse, the result of an elastic collision, or, secondly, long double pulses, the result of double impact or, thirdly, an oscillating plateau pulse indicative of a particle rolling along the electrode. These types of pulse are all distinctly shown in Figure 2 (see also [19]).

The distinction in pulse values for particles of the same size shows that the contact time during collision, τ_c, which is indirectly proportional to frequency to a first approximation [20], is not equal in each specific instance. The existence of indirect contacts [19] is caused by the fact that not all the particles, especially at small degrees of fluidization, have a velocity sufficient for elastic collision. Small particles ($d_p < 0.5$ mm) are also inclined to aggregation [2].

The values of individual collision frequencies for glass particles of various fractions lay in the region of 10 Hz. Frequency increased with increase in particle size (Figure 3(a)). This is caused by the increase in the average velocity of particle movement with increase in diameter [21, 22] at the same porosity, as greater flow velocities are needed for fluidization of the larger particles. However, collision frequency per unit electrode area decreases with increase in particle diameter (Figure 3(b)), as the number of particles per unit electrode area, n_s, is indirectly proportional to diameter squared [23]:

$$n_c = 1/L^{2/3} d_p^2 \tag{2}$$

Mass transfer to the electrode may be attributed to two effects: (i) the current at minimum fluidization and (ii) the current caused by collisions (Figure 4):

$$i_d = i_{mf} + i_c \tag{3}$$

In the packed bed regime collisions are absent. The increase in limiting diffusion current with increase in flow velocity is caused by the increase in flow velocity within the bed, the so-called interstitial velocity, U_{in}. The particles act as mobile turbulizers. The U_{in} in the bed is much higher than that outside the bed, U [7]. U_{in} reaches its maximum magnitude at minimum fluidization, when $U = U_{mf}$, and remains practically constant within the flow rate range corresponding to the 'dense' fluidized bed regime at $0.45 < \varepsilon < 0.65$ (Figure 4).

Upon bed expansion the currents increase relative to that for minimum fluidization, and the region of diffusion control is shifted to higher overvoltages. Diffusion currents reach a maximum in the porosity range $0.5 < \varepsilon < 0.6$, and then fall towards values corresponding to $\varepsilon \to 1$ (empty channel flow) [2, 9].

Thus, the influence of U_{in} on the limiting diffusion current remains constant, so $i_{in} \equiv i_{mf}$. The interstitial velocity, U_{in}, for each particle diameter can be determined via the appropriate minimum fluidization velocity on comparison of limiting currents in a channel without particles and in a FIB (Figure 4) according to the equation:

$$U_{in} = U_{mf}(i_{mf}/i_{ec}^{mf}) \tag{4}$$

U_{mf} can be found experimentally (Figure 5), or calculated from the equation (see Appendix):

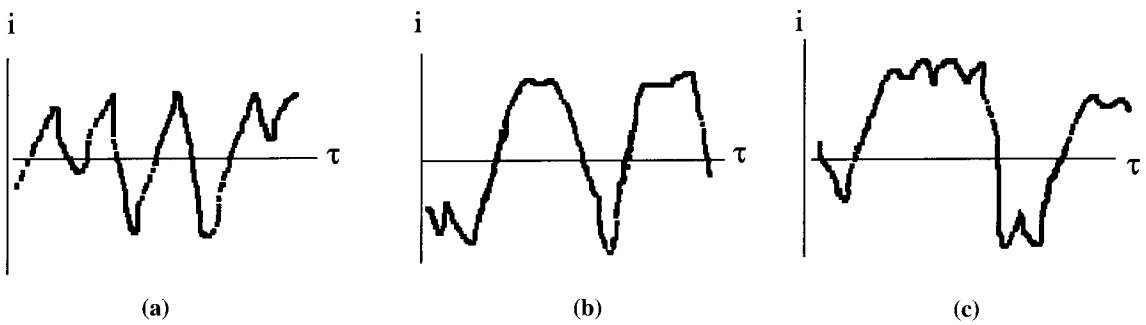

Fig. 2. Characteristic oscillogrammes of collision currents. (a) single peaks; (b) double peaks; (c) rolling of particles.

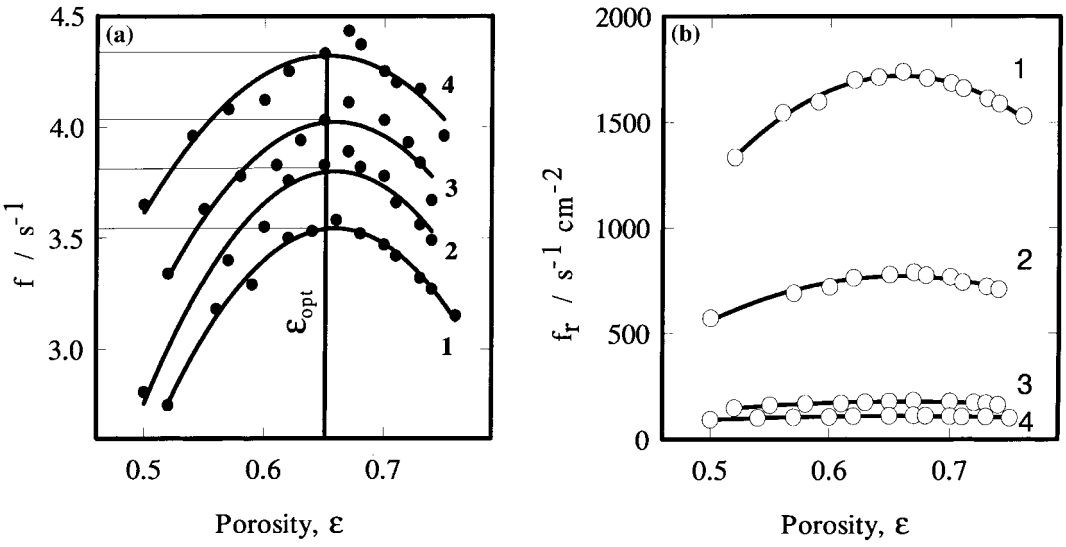

Fig. 3. Dependence of collision frequency on the bed porosity. (a) Frequency of individual collisions; (b) collision frequency per unit area. (1–4) $d_p = 0.057$, 0.072, 0.16 and 0.225 cm, respectively.

$$U_{mf} = \left[\frac{4}{3}\frac{g(\rho_p - \rho_s)}{\xi\rho_s}d_p\right]^{1/2} \tag{5}$$

The additional mass-transfer enhancement occurs due to particle collisions with the electrode.

As the porosity of a packed bed is independent of particle diameter [10], the merging of the rising sections may be expected for curves □, △ and ▽ for the planar electrode in Figure 6. However, each particle is surrounded by a hydrodynamic boundary layer [6]. The influence of the hydrodynamic layer on intrinsic porosity increases with reduction in particle diameter [24]. The real flow velocity between the particles and over the electrode increases. This results in a more abrupt increase in limiting diffusion currents in the beds containing the smallest particles.

The geometric voidage between particles increases with increasing particle diameter, and the influence of the hydrodynamic layer on local flow velocity and on limiting current values decreases (Figure 6). To find that part of the limiting diffusion current caused by collisions, i_c, and its dependence on particle size, it is necessary to discuss the influence of the collision mechanism on the electrode process.

Upon collision the particles introduce a total microvolume $\Sigma\Delta V$ per unit time per unit electrode area. This is equal to the product of the specific microvolume, ΔV, and the collision frequency f_r:

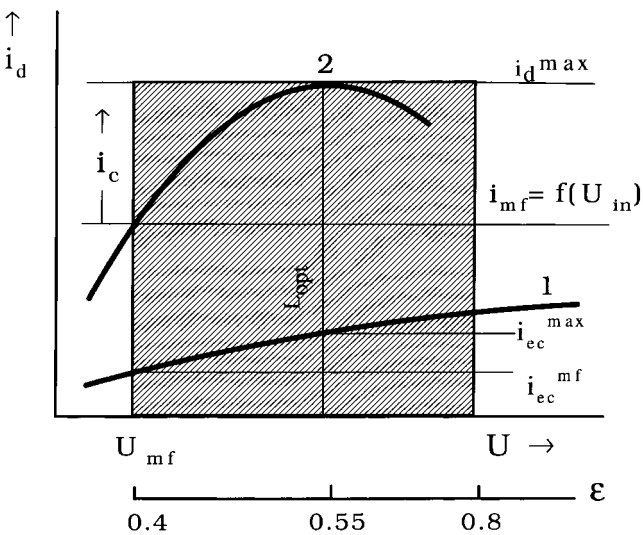

Fig. 4. Scheme for limiting diffusion current calculations. (1) Mass transfer in flow without particles; (2) mass transfer in FIB.

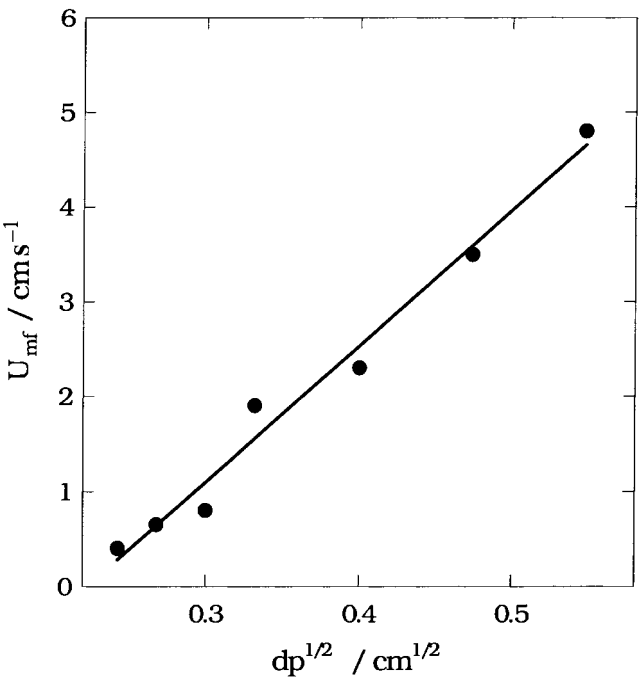

Fig. 5. Dependence of minimum fluidization velocity, U_{mf}, on particle size.

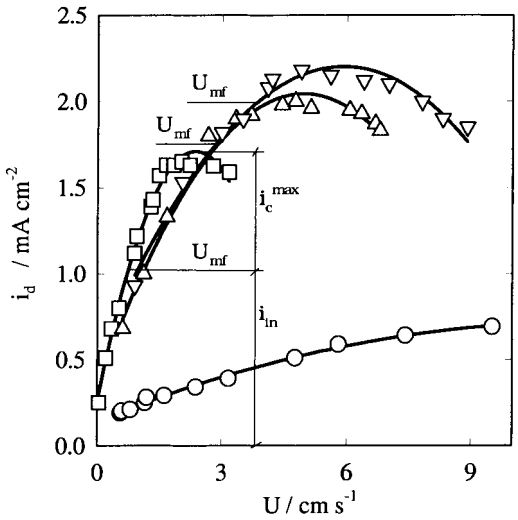

Fig. 6. Dependence of limiting diffusion currents for copper ion electroreduction at a planar electrode on electrolyte flow velocity. $\rho_p = 2.5\,\mathrm{g\,cm^{-3}}$. $[Cu^{2+}] = 3.15 \times 10^{-3}$ M. Key: (○) mass transfer in flow without particles; mass transfer in FIB: (□) $d_p = 0.08$; (△) $d_p = 0.16$ and (▽) $d_p = 0.25$ cm, respectively.

$$\Sigma\Delta V = f_r\ \Delta V \tag{6}$$

The value of the specific microvolume, ΔV, introduced into the diffusion layer by a single particle is approximately equal to the volume of a spherical segment having $h = \delta$ and diameter, d_{eff}, equal to the diameter of the particle together with its hydrodynamic boundary layer (Figure 7). A microvolume of electrolyte is brought into the near electrode layer during particle movement towards an electrode. Considering [2, 6], that for most aqueous electrolytes, $\delta_o \approx 10\delta$, we can write:

$$\Delta V = \pi\delta^2\left[(0.5d_p + 10\delta) - \delta/3\right] \tag{7}$$

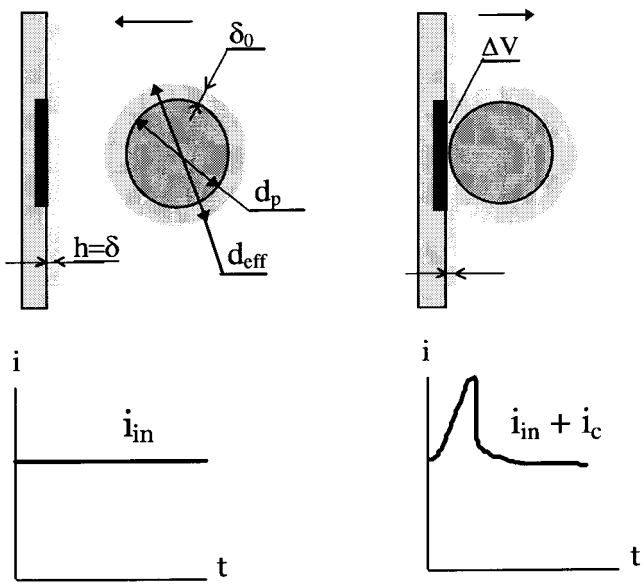

Fig. 7. Model of particle collision with the electrode.

The diffusion layer thickness, δ, is calculated taking into account the assumption that interstitial flow velocity at the electrode is equal to that for the bulk particle region. At minimum fluidization, the appropriate values of limiting current, i_{mf}, (Figure 4) are related to the diffusion layer thickness by the equation:

$$i_{mf} = zFc_oD/\delta \tag{8}$$

Hence,

$$\delta = zFc_oD/i_{mf} \tag{9}$$

The dependence of the diffusion layer thickness on particle diameter in cm (Figure 8) may be described by the empirical equation [24]:

$$\delta = 5.88 \times 10^{-4}\, d_p^{-1/2} \tag{10}$$

The thickness of the effective near-electrode diffusion layer for particles of various sizes was calculated according to Equation 10. The i_{mf} values for 0.8 mm $> d_p >$ 2.5 mm particles were determined experimentally and, for particles of smaller size, were calculated from the data [12] employing i_{mf} calculated from Equation 8. The diffusion coefficient for copper ions at 293 K was taken as $D_{Cu^{2+}} = 3.95 \times 10^{-6}\ \mathrm{cm^2\,s^{-1}}$ [25].

Assuming that Cu^{2+} ions, penetrating the diffusion layer during collision, are completely consumed in electrochemical reaction, the collision currents may be calculated from the equation:

$$i_c = zFc_o\ f_r\ \Sigma\Delta V \tag{11}$$

The dependence of collision current values on average particle diameter at a microelectrode, calculated on the

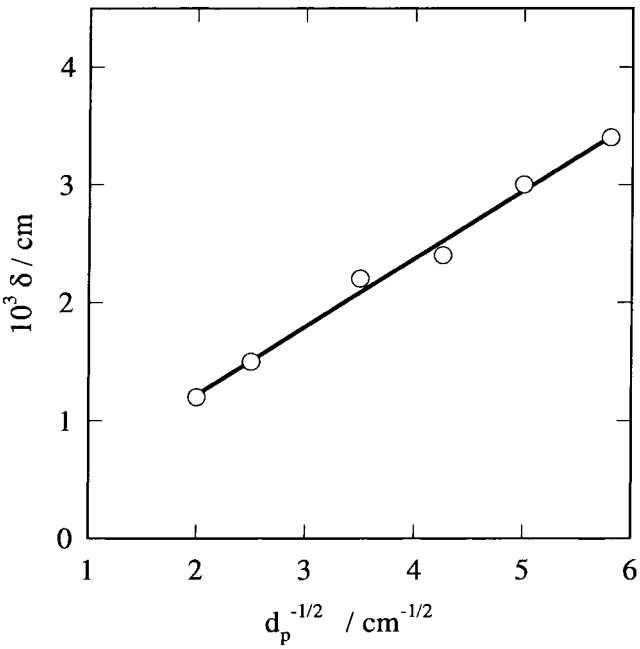

Fig. 8. Dependence of diffusion layer thickness on particle diameter.

basis of the proposed model, is shown in Figure 9. The i_c values are proportional to the inverse of the square of the particle diameter.

Collision currents were also calculated from current against electrolyte velocity dependencies (Figure 6) at the maximum values of limiting current. The reasonable agreement between the collision current values found by two independent methods confirms the model. Some discrepancy in i_c values may be explained by the fact that, as outlined in [19], the real time of contact may differ from that suggested in [20].

Maximum limiting current values (Figure 6) correspond to the optimum degree of bed expansion and coincide with maximum average particle kinetic energy values [21, 22] and collision frequencies (Figure 3). The occurrence of these maxima [23], is caused by the interaction of several factors related to the increase in flow velocity and the increase in average particle movement with the degree of bed expansion, and the decrease in collision frequency.

The i_c values were also calculated for each average particle diameter of the studied fractions from the values of current pulses on oscilloscope traces from the equation:

$$i_c = 0.707 A_c / R_{met} S_e \tag{12}$$

The values of i_c from the two methods agree in order of magnitude (from 7.2 to 4.6 mA cm^{-2} depending on d_p), and decrease with increase in particle diameter. The magnitude of the oscilloscope signal depends linearly on ionic concentration (Figure 10). The values of the oscilloscope pulse, registered in beds of different size fractions, are not equal; this effect is caused, according to Equation 7, by the differences in electrolyte microvolumes, ΔV, introduced. With increase in particle diameter the microvolume of electrolyte increases, but simultaneously the collision frequency is sharply reduced. Therefore, the contribution of a collision current to mass-transfer to a macroelectrode diminishes with increase in particle size. This additionally confirms the validity of the model.

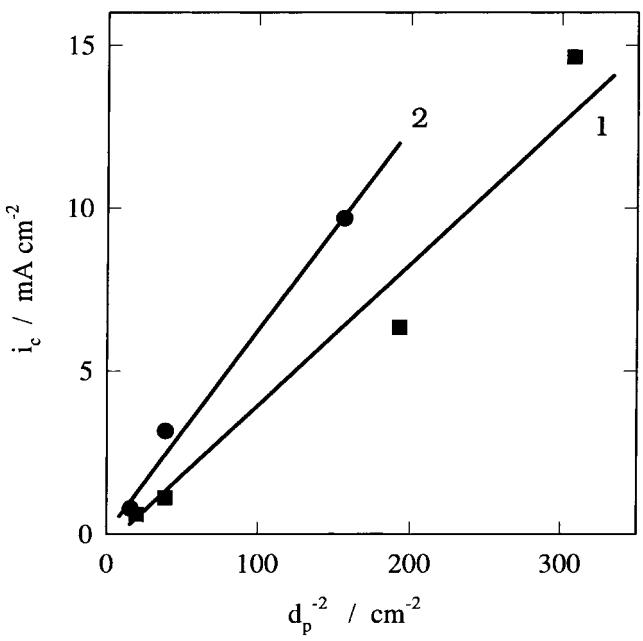

Fig. 9. Dependence of collision current values at a microelectrode on particle diameter. Key: (1) data, calculated according to Equation 11; (2) from current-electrolyte flow velocity, dependencies (Figure 4). $[Cu^{2+}] = 5 \times 10^{-2}$ M.

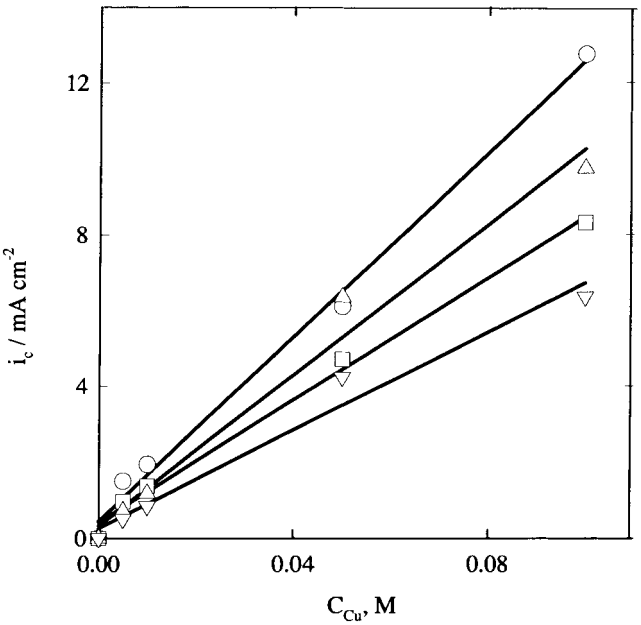

Fig. 10. Dependence of current values, calculated from oscilloscopic pulses at a microelectrode on the concentration of the discharged ion $L = L_{opt} = 1.5$, $R_{met} = 10.5$ kΩ. Key: (○, △) maximum magnitudes of collision currents; (□, ▽) average magnitudes of collision currents; (○, □) microelectrode diameter 0.169 cm, $d_p = 0.16$ cm; (△, ▽) microelectrode diameter 0.094 cm; $d_p = 0.11$ cm.

The mass-transfer rate at the macreoelectrode in a FIB increases with increase in particle diameter (Figure 6). Enhancement of mass-transfer rate occurs as the result of growth of the contribution caused by U_{in}, as the increase in d_p results in increase in U_{mf} (Equation 5). Simultaneously, the increase in U_{in}, with increase in d_p results, on the one hand, in thinning of the boundary layer, δ, which results in decrease in fluid microvolume, ΔV (Equation 7). On the other hand, the number of particles per unit volume decreases (Equation 2). Finally a decrease in the contribution of collision currents to the mass-transfer rate to the macroelectrode takes place (Figure 11). The dependence i_c/i_d against $d_p^{-3/2}$ is explained by the fact that, under the considered conditions, $i_d \sim d_p^{1/2}$ [24], while $i_c \sim d_p^{-2}$ (Figure 9).

The existence of collision currents explains previous results [8], where the influence of glass beads on limiting current values for electrochemical reduction of ferricyanide ions at a rotating disc electrode was investigated. It was shown that a 7.5 fold increase in rotation rate (from 40.5 up to 300.5 rad s^{-1}) produced an increase in mass transfer rate corresponding to a diffusion layer

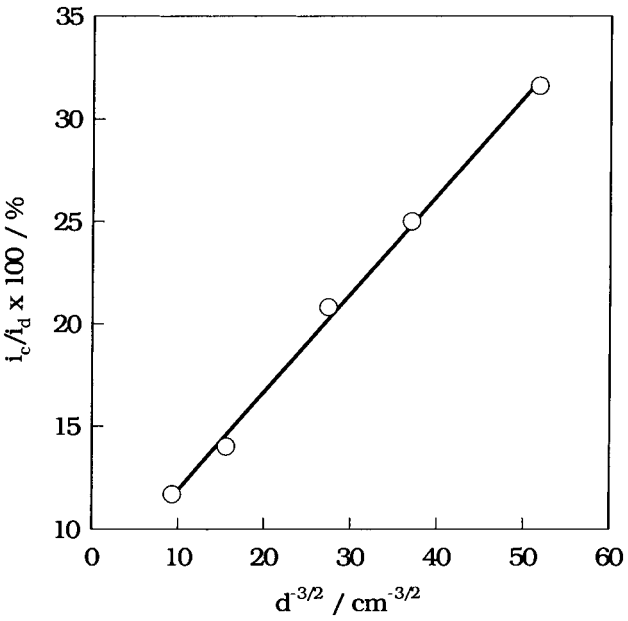

Fig. 11. Dependence of the ratio of the collision current contribution, i_c, at a macroelectrode to the total current value, i_d, on particle diameter. $L = L_{opt}$.

thickness decrease of only 2.3 fold in the absence of inert packing. For particles (sand, glass beads etc.) suspended by stirring, the mass transfer rate increased more than eight times in the same range of electrode rotation rates. This positive effect was achieved due to diffusion layer renewal, resulting from particle contact with the electrode. As in an FIB where an optimum degree of expansion exists, the optimum volumetric concentration of the solid phase in this latter case was of the order of 40%.

The existence of such an optimum in both cases may be explained by the competition between two factors, namely, increase in the average particle kinetic energy and reduction in the collision frequency with increase in fluidized or stirred bed expansion. The latter is caused by the restriction of movement of suspended particles with increase in their volumetric concentration.

4. Conclusions

A model describing the influence of particle-wall collisions on the mass transfer rate mechanism in fluidized inert bed electrochemical cells is proposed. The values of the collision current contribution, i_c, to mass transfer to electrodes in fluidized beds of inert particles can be calculated from the proposed model and compared to those obtained from experimental data. The values of i_c obtained by the two independent methods are in good agreement.

In accordance with the proposed model, at each collision a defined microvolume of electrolyte penetrates the near-electrode diffusion layer, thus causing enhancement of the limiting diffusion current. The mass transfer contribution due to electrolyte flow velocity increases with increase in particle diameter; while that due to particle collision decreases. The general mass transfer rate increases with increase in particle diameter following the relationship $i_d = f(d_p^{1/2})$.

Thus, the contribution of particle collision currents to mass transfer to an electrode in a FIB can be quantitatively estimated, taking into account the effective particle size in a viscous (nonideal) liquid.

References

1. H. Bloom and F. Gootman (eds), '*Electrochemistry. The Past Thirty and the Next Thirty Years*' (Plenum Press, New York, 1977).
2. P. le Goff, F. Vergnes, F. Coeuret and J. Bordet, *Ind. & Eng. Chem.* **61** (1969) 8.
3. BEWT (Water Engineers Ltd) Industrial Literature, Tything Road, Arden Forest Industrial Estate, Alcester, Warwickshire, D49 6ES, UK.
4. 'TEMP' Amalgamation, '*The Catalogue of Productions*', 1991–1996, Khmelnitskii, 280000, Mir Avenue, 99–101, Ukraine.
5. W.W. Focke, *Electrochim. Acta* **28** (1983) 1137.
6. B. Levich, '*Physicochemical Hydrodynamics*', (Prentice Hall, NY, 1st edn, 1964).
7. N.A. Shvab, A.V. Gorodyskii and V.A. Sobkevich, *Elektrokhimiya* **19** (1983) 800.
8. R.H. Muller, D.J. Roha and C.W. Tobias, *in* R.S. Yed, T. Katan and D.-T. Chin (eds), '*Transport Processes in Electrochemical Systems*', (Electrochemical Society, Pennington, NJ, 1982), Part I.
9. N.A. Shvab, N.V. Stefanjak, E.I. Kondruk, V.A. Sobkevich and K.A. Kazdobin, *Ukr. Khim. Zh.* **56** (1990) 1057.
10. D.C. Carbin and D.R. Gabe, *Electrochim. Acta* **19** (1974) 645.
11. L.M. Kovacs, *Period. Polytechn. Chem. Eng.* **24** (1980) 171.
12. A.T.S. Walker and A.A. Wragg, *Electrochim. Acta* **25** (1980) 323.
13. K. Bouzek, J. Palmer, I. Rousar and A.A. Wragg, *Electrochim. Acta* **41** (1996) 583.
14. A. Storck and F. Coeuret, *Can. J. Chem. Eng.* **55** (1977) 427.
15. N.A. Shvab and N.V. Stefanjak, *Ukr. Khim. Zh.* **52** (1986) 211.
16. H. Kametani, *Jap. Chem. Eng.* **13** (1974) 201.
17. J. Held and H. Gerischer, *Ber. Bunsenges. Phys. Chem.* **67** (1963) 921.
18. A.A.C.M. Beenackers, W.P.M. van Swaaij and A. Welmers, *Electrochim. Acta* **22** (1977) 1277.
19. Y. Sakai, H. Unno and T. Akehata, 3rd World Congress of Chemical Engineering, Tokyo, 1986, **2** (21–25 Sept. 1986) 435.
20. R.M. Lazorenko-Manevich and A.V. Ushakov, *Doklady Akademii Nauk USSR* **161** (1965) 156.
21. J. Bordet, P. le Goff and F. Vergnes, *Powder Technol.* **5** (1971/72) 365.
22. J. Bordet, O. Borlai, F. Vergnes and P. le Goff, *Inst. Chem. Eng. Symp. Ser.* **30** (1968) 165.
23. M. Fleishmann and J.W. Oldfield, *J. Electroanal. Chem.* **29** (1971) 231.
24. N.A. Shvab, *Ukr. Khim. Zh.* **51** (1985) 622.
25. J.R. Burrows, J.A. Harrison and J. Thompson, *J. Electroanal. Chem.* **58** (1975) 241.

Appendix

Equation 5 is based on an equilibrium force balance involving the gravity, buoyancy and drag forces at the moment of fluidization. The equation indicates the relationship $U_{mf} = f(d_p^{1/2})$. This form of relationship

was obtained experimentally and can also be substantiated theoretically.

At $U = U_{mf}$ an equilibrium force balance involving G, the gravity force, B the buoyancy force and D the drag force on a particle can be drawn up:

$$D = G - B$$

Now, $G = \pi g d_p^3 \rho_p / 6$ and $B = \pi g d_p^3 \rho_s / 6$, therefore the drag force, is given by

$$D = \xi A_p U_{mf}^2 \rho_s / 2$$

where ξ is the drag coefficient and A_p is the maximum cross section of a particle (i.e., $A_p = \pi d_p^2 / 4$).

Thus,

$$D = \xi \pi d_p^2 U_{mf}^2 \rho_s / 8$$

So, balancing the forces leads to the following:

$$(\xi \pi d_p^2 U_{mf}^2 \rho_s / 8) = (\pi g d_p^3 \rho_p / 6) - (\pi g d_p^3 \rho_s / 6)$$

which gives

$$U_{mf}^2 = \frac{4}{3} g d_p \frac{(\rho_p - \rho_s)}{\rho_s \xi}$$

and thus,

$$U_{mf} = f(d_p^{1/2})$$